The Budyko and complementary relationships in an idealized model of large-scale land-atmosphere coupling

Benjamin R. Lintner[1]*, Pierre Gentine[2], Kirsten L. Findell[3], and Guido D. Salvucci[4]

In preparation for Hydrology and Earth Systems Science

18 February 2015

[1]*Department of Environmental Sciences, Rutgers, The State University of New Jersey, New Brunswick, NJ, USA*

[2]*Department of Earth and Environmental Engineering and Earth Institute, Columbia University, New York, NY, USA*

[3]*Geophysical Fluid Dynamics Laboratory, Princeton, NJ, USA*

[4]*Department of Earth and Environment, Boston University, Boston, MA, USA*

---

*Corresponding author: Benjamin R. Lintner, Department of Environmental Sciences, Rutgers, The State University of New Jersey, 14 College Farm Road, New Brunswick, NJ 08901-8551, USA

Email: lintner@envsci.rutgers.edu

Telephone: (848) 932-5731

Abstract.

Two well-known relationships in hydrology and hydrometeorology, the Budyko and complementary relationships, are examined within an idealized prototype representing the physics of large-scale land-atmosphere coupling developed in prior work. These relationships are shown to hold on long (climatologic) time scales because of the tight coupling that exists between precipitation, atmospheric radiation, moisture convergence and advection. The slope of the CR is shown to be dependent the Clausius-Clapeyron relationship between saturation specific humidity and temperature, with important implications for the continental hydrologic cycle in a warming climate, e.g., one consequence of this dependence is that the CR may be expected to become more asymmetric with warming, as higher values of the slope imply a larger change in potential evaporation for a given change in evapotranspiration. In addition, the transparent physics of the prototype permits diagnosis of the sensitivity of the Budyko and complementary relationships to various atmospheric and land surface processes. Here, the impacts of anthropogenic influences, including large-scale irrigation and global warming, are assessed.

1) Introduction

Observations of the annual terrestrial surface water balance demonstrate a tight and relatively simple functional dependence of evapotranspiration on the atmospheric water supply (precipitation) and demand (potential evaporation) at the surface (Budyko 1961, Porporato et al. 2004, Roderick and Farquahr 2011, Williams et al. 2012, Zanardo et al. 2012). Such observations have stimulated development of simplified analytical formulations of the annual water balance (Budyko, 1961; Lettau, 1961; Eagleson 1978a, 1978b, 1978c; Fu 1981; Milly 1994; Porporato et al. 2004; Harman et al. 2011; Sivapalan et al. 2011). Budyko (1961, 1974) developed arguably the most well-known approach for characterizing catchment-scale hydrologic balances on long (decadal and greater) timescales. By hypothesizing limitations on land surface evapotranspiration imposed by the availability of water and energy, Budyko introduced a relationship of the form:

$$\frac{E}{P} = B\left(\frac{E_p}{P}\right) \tag{1}$$

where E, P, and E_p are evapotranspiration, potential evapotranspiration, and precipitation, respectively. The ratio E_p/P is commonly known as the dryness or aridity index (ϕ), and hereafter we denote the ratio E/P as $B(\phi)$, i.e., the Budyko curve. Empirical forms of $B(\phi)$ have been obtained by fitting to observed E, P, and E_p with E typically estimated as the residual of precipitation and basin-scale streamflow (Budyko 1961, 1974). $B(\phi)$ appears to be rather stable across different regions and hydroclimatic environments (Potter et al. 2005; Yang et al. 2007; Gentine et al. 2012).

The last two decades have seen renewed interest in the Budyko curve (e.g., Milly 1994; Koster and Suarez 1999; Milly and Dunne 2002; Porporato et al. 2004; Potter et al. 2005; Donohue et al. 2007; Yang et al. 2008; Gerrits et al. 2009; Gentine et al. 2012; Istanbulluoglu et

al. 2012; Williams et al. 2012). Many studies have employed simplified models of the surface and groundwater moisture response to precipitation forced by E_p to investigate the robustness of the Budyko curve in different catchments. Milly (1994) and Porporato et al. (2004), in particular, investigated the response of the annual water balance to changes in the characteristics of potential evaporation and precipitation intensity and frequency yielding new insights on the sensitivity of the annual water balance to changes in surface energy and water forcing, all other factors, e.g., vegetation characteristics, soil, topography, remaining constant. However, apart from a few studies investigating the catchment co-evolution and adaptation of vegetation to the water and energy forcing (Troch et al. 2009; Sivapalan et al. 2011; Gentine et al. 2012), a direct explanation of the stability and widespread applicability of the Budyko relationship across a range of conditions remains elusive.

In the Budyko framework, as in most hydrologic models, E_p is prescribed as a forcing, which is thought to be independent from the surface. Nonetheless, E and E_p have been hypothesized to be inversely related to one another (Bouchet 1963; Morton 1983; Brutsaert and Stricker 1979; Hobbins et al. 2001) on daily to annual time scales. In fact, the coupling between E and E_p provides the basis for a foundational relationship in hydrometeorology: the complementary relationship, first introduced by Bouchet (1963) and Morton (1983). Mathematically, the complementary relationship (CR) can be expressed as:

$$E_p + bE = (1 + b)E_{wet} \, . \tag{2}$$

In (2), E_p is potential evaporation and E_{wet} is the energy-limited, wet surface equilibrium evapotranspiration. Bouchet (1963) assumed a value of 1 for the scale factor b while Pettijohn and Salvucci (2009), hereafter PS09, report values in the range 3-6 based on numerical

simulations of an evaporation pan in a drying environment. Since E_p cannot directly be measured, pan evaporation has often been used in lieu of potential evaporation using a pan correction factor (Bosman 1987, Roderick and Farquahr 2004; van Heerwaarden et al. 2010). Kahler and Brutsaert (2006) assumed that use of pan measurements in equation (2) may account for $b > 1$ because a pan transmits heat, resulting in warmer water inside the pan relative to a larger free water body (e.g., lake) under similar ambient conditions.

Although several studies (Zhang et al. 2004; Ramirez et al. 2005; Szilagyi and Jozsa 2009) have discussed possible links between the CR and the Budyko curve, to date a theoretical framework encompassing either or both of these relationships is still absent. Milly (1994) underscores the lack of physical understanding for why the Budyko curve deviates from its water- and energy-limited asymptotes, while Ramirez et al. (2005) suggest that, apart from heuristic arguments or under restrictive conditions, no general proof of the CR is available. Moreover, questions remain about the applicability and validity of the Budyko and complementary relationships across different spatial and temporal scales. Here we note that observational data confirm the CR holds on daily to annual time scales (Bouchet 1963; Kahler and Brutsaert 2006) and across local to regional spatial scales (Granger 1989, Szilagyi 2001; Crago and Crowley 2005; PS09; van Heerwaarden et al. 2010), which is usually understood in terms of the diurnal-scale interactions of the boundary layer with the surface, although questions have been raised about some of the assumptions inherent in these approaches. Indeed, as PS09 note, some explanations for the CR have relied on contradictory assumptions. For example, the derivation of Szilagyi (2001) assumes that as E decreases, the surface temperature of the evaporation pan remains constant while the overlying near surface specific humidity decreases, increasing the vapor deficit and thus the evaporation rate over the pan. By contrast, in Granger

106 (1989) surface temperature is assumed to increase while specific humidity remains constant, thus
107 also increasing the humidity gradient and pan evaporation rate. Lhomme and Guilioni (2006)
108 have questioned the physical validity and applicability of these assumptions.

109 In the present study, we make use of a semi-analytic, idealized prototype of large-scale land-
110 atmosphere coupling developed in prior work (Lintner et al. 2013) to derive the Budyko and
111 complementary relationships. Our approach differs from prior analyses in that: (i) it is implicitly
112 large-scale and relevant on climatic timescales; and (ii) convergence, advection, precipitation
113 and atmospheric radiation are treated implicitly rather than as exogenous forcing. The latter
114 renders the atmospheric and surface moisture interactive and tightly coupled vertically but also
115 horizontally—through the (nonlocal) effects of moisture advection and convergence. Several
116 studies have pointed out that such tight coupling between radiation, larger-scale circulation and
117 local surface energy budget is key to understanding locally-observed land-atmosphere
118 interactions (Betts et al. 1996; 2003; Betts and Viterbo 2005; Betts 2007a; 2014). The analytic
119 simplicity of the idealized prototype facilitates straightforward diagnosis of factors influencing
120 the large-scale coupling, as highlighted in Lintner et al. (2013).

121 A key motivation for this study is consideration of how the continental hydrologic cycle, and
122 more precisely how the behavior reflected in the Budyko curve and CR, may respond to
123 anthropogenic influences. Indeed, the projected response of terrestrial hydrologic cycle to
124 various climate change mechanisms in models remains subject to large uncertainties (Sherwood
125 and Fu 2014). Emergent behaviors such as the Budyko and complementary relationships may
126 provide useful constraints on such uncertainties. For example, Brutsaert and Parlange (1998)
127 have suggested that the CR may explain the apparent paradox between observed downward

128 trends in pan evapotranspiration over the late 20th century and anticipated increases in
129 evaporation resulting from a more intense hydrologic cycle in a warming atmosphere.

130 The paper is organized as follows. After providing a brief review of the prototype
131 assumptions and governing equations (Section 2), we analyze the generalized Budyko and
132 complementary relationships within our prototype (Section 3) and consider the physical
133 parameters and processes impacting these relationships (Section 4). Here we are interested in
134 examining the behavior across a range of hydroclimatic states; in what follows, we use the term
135 "prototype transect" to refer to this range. This may be viewed as representing either a spatial
136 sampling of states across a climatological gradient in soil moisture at a fixed point in time or a
137 temporal sampling (as under the seasonal evolution) at a fixed point in space. In Section 5, we
138 examine how anthropogenic influences such as global warming and large-scale irrigation affect
139 these relationships.

140

141 **2) Overview of the idealized land-atmosphere coupling prototype**

142 In prior work (Lintner et al. 2013), we developed a semi-analytic prototype for land-atmosphere
143 coupling. This prototype describes the coupling at spatial scales for which both local
144 (evapotranspiration) and nonlocal processes (horizontal moisture advection and convergence)
145 may be important to the water cycle budget. We consider steady-state conditions, corresponding
146 to the climatological state of the hydrologic cycle. Although the steady-state assumption clearly
147 limits the applicability of our model in the presence of important time-dependent processes
148 operating in the climate system, we again note that the CR has been observed to hold across a
149 range of timescales. Similarly Budyko curves have been estimated from yearly mean
150 observations (Budyko 1974, Gentine et al. 2012).

151 The atmospheric component of this prototype is based on vertically-integrated
152 tropospheric temperature and moisture equations from the Quasi-equilibrium Tropical
153 Circulation Model (QTCM; Neelin and Zeng 2000; Zeng et al. 2000), an intermediate level
154 complexity model for the tropical atmosphere:

155 $$-Ms\nabla_H \cdot \mathbf{v} + P + R_{net} + H = 0 \quad (3)$$

156 $$Mq\nabla_H \cdot \mathbf{v} - P + E - \mathbf{v_q} \cdot \nabla_H q = 0 \quad (4)$$

157 where ∇_H is the horizontal gradient operator; R_{net} is the net column (top of the atmosphere
158 minus surface) radiative heating; Ms and Mq are the dry static stability and moisture
159 stratification and $\nabla_H \cdot \mathbf{v}$ is signed positive for low-level convergence; and $\mathbf{v_q}$ is the vertically-
160 averaged horizontal wind vector weighted by the moisture vertical structure assumed in QTCM1.
161 (Note that baseline values for parameters such as Ms and Mq are given in Lintner et al. 2013 and
162 references therein. Table 1 summarizes parameter values most relevant to the present study.)
163 The term P in (3) and (4) represents the net convective (condensational) heating and drying,
164 respectively; the negative sign in (4) indicates that precipitation is a net sink of vertically-
165 averaged tropospheric moisture. For the temperature equation (3), we have neglected horizontal
166 temperature gradients following the weak temperature gradient assumption (Sobel and
167 Bretherton 2000; Sobel et al. 2001). Note that all terms appearing in (3) and (4) are implicitly
168 scaled to units of mm day^{-1} by absorbing constants such as (specific) heat capacity, latent heat of
169 fusion, and column mass per unit area $\Delta p/g$, where Δp is the tropospheric pressure depth.

170 A steady balanced surface energy flux constraint, in which the annual-mean ground
171 surface heat flux is neglected, reads:

172 $$R_{surf} - E - H = 0 \quad (5)$$

173 where the net surface radiative heating, R_{surf}, is signed positive downward.

In Lintner et al. (2013), we consider tropospheric temperature (T) as prescribed and solve the system of equations (3)-(5) for q, $\nabla_H \cdot \mathbf{v}$, and surface temperature Ts for prescribed large-scale advection. A closed-form, self-consistent solution can be obtained by invoking the steady-state soil moisture budget:

$$P - E - Q_{runoff} = 0 \tag{6}$$

where Q_{runoff} is the net runoff. For analytic simplicity, we assume a simple bucket model, with an evaporative efficiency, $\beta = \frac{E}{E_p}$, for which we assume a simple linear relationship $\beta = w$ (Porporato et al. 2001, 2004), where w is the dimensionless soil moisture (actual soil moisture normalized by a holding capacity). Q_{runoff} is represented as the precipitation rate times a power law of soil moisture, $Q_{runoff} = Pw^{\eta}$ (Kirchner 2009). The baseline power law scaling exponent is $\eta = 4$, the value used in Lintner et al. (2013). The suitability of invoking a single moisture storage variable to represent both basin scale evaporative efficiency and runoff has recently been demonstrated at nine watersheds containing Ameriflux eddy covariance measurements of evaporation and gauged streamflow (Tuttle and Salvucci, 2012).

For analytic simplicity, we consider linearized radiative and surface turbulent fluxes of the form:

$$\begin{aligned} H &= H_0 + \varepsilon_H(Ts - a_{1s}T) \\ E &= \beta[Ep_0 + \varepsilon_H(\gamma Ts - b_{1s}q) \\ R_x &= R_{x0} + \varepsilon_{Ts}^{Rx}Ts + \varepsilon_T^{Rx}T + \varepsilon_q^{Rx}q + c_xP \end{aligned} \tag{7}$$

Quantities with subscript "0" denote the values about which the fluxes are linearized, with coefficients ε representing the linear sensitivity of fluxes to T, q, and Ts. The scale factors a_{1s} and b_{1s} relate vertically-averaged temperature and moisture to near surface values appropriate

for computation of surface bulk turbulent fluxes. The coefficient $\gamma = \frac{dq*}{dT}$ is the slope of the saturation specific humidity (q^*) with respect to temperature, as defined via the Clausius-Clapeyron equation. Note that in our usage, q (or q^*) is implicitly scaled to units of temperature (K) via absorption of the psychrometric constant; thus γ is dimensionless. The radiative fluxes are calculated at the top-of-the-atmosphere and the surface ($x = toa$ and $x = surf$), and the coefficients c_x are cloud-radiative forcing sensitivities, with cloud-radiative fluxes assumed to be linearly proportional to the precipitation rate. Precipitation (convective heating in equation (3) or convective drying in equation (4)) is formulated in terms of a Betts and Miller (1986)-type relaxation scheme:

$$P = \max\left[\varepsilon_c\left(q - q_c(T)\right), 0\right]. \quad (8)$$

Here, $q_c(T)$ is a temperature-dependent moisture threshold and ε_c is the convective adjustment rate coefficient (inversely related to the timescale for convective adjustment τ_c).

3) Overview of the baseline relationships

3a) Complementary relationship

Figure 1a illustrates the functional relationships between soil moisture and E, P, and E_p of the prototype. The general response of E and E_p with increasing soil moisture, namely E_p decreasing and E (generally) increasing, is consistent with the CR (2). E_p relates to w through the deficit between ambient and saturation specific humidity at the surface (Lintner et al. 2013): the deficit decreases with increasing soil moisture since q increases and Ts decreases. Figure 2 depicts the results of the prototype against E and E_p observations from Little Washita River Basin near Chickasha, Oklahoma (see Kahler and Brutsaert 2006 for a full description of the dataset). Here

217 E_p was obtained directly from pan evaporation measurements with a correction factor and E was
218 measured using the Bowen ratio (EBBR) technique. E and E_p are presented in dimensionless
219 units by dividing by the Priestly and Taylor (1972) evaporation, i.e., $E_{wet} = \alpha \frac{\gamma}{1+\gamma} R_{surf}$, where
220 α is a correction factor with an estimated value of ~1.26. The CR from the prototype shows a
221 qualitative, and arguably even quantitative, correspondence with both observational datasets. Of
222 course, we should point out that the prototype was not explicitly tuned to represent the
223 hydroclimate of these locations, and as such, any quantitative correspondence may be
224 coincidental. Moreover, the scatter inherent in the observations would permit a range of
225 plausible complementary relationships.

226 A slight decrease in E is observed for $w \gtrsim 0.7$ (see the gray curve in Figure 1a). To our
227 knowledge such a decrease has not been previously investigated, even though it appears in *in situ*
228 measurements (Kahler and Brutsaert 2006; PS09), as evident in Figure 2. The decrease of both
229 E and E_p arises from the monotonic decrease in E_p ($\frac{\partial E_p}{\partial w} < 0$) at large soil moisture, as pointed
230 out by Lintner et al. (2013). Indeed, in the prototype, increasing soil moisture is a consequence of
231 increasing precipitation, with the latter progressively balanced by higher moisture convergence
232 (c.f., Figure 3 of Lintner et al. 2013). Increasing moisture convergence is associated with
233 increasing (low-level) humidity, which reduces the surface vapor pressure deficit, thereby
234 reducing E_p. Overall the moisture balance at large soil moisture values implies a greater role for
235 nonlocal processes. On the other hand, at very low soil moisture values, mean P is mostly
236 balanced by E, resulting in a tight link among E, E_p, and w. This explains the success of local
237 coupled land-boundary layer models (Bouchet 1963, van Heerwarden et al. 2010) in representing
238 the drier regime of the CR.

239 In prior studies of the CR, a quantity E_{wet} is introduced to denote the point of convergence of
240 E and E_p under unlimited soil moisture (saturated surface) conditions i.e. at high soil moisture
241 values (see equation 2). Conventionally, E_{wet} is assumed to represent equilibrium E from a
242 saturated surface when advection is minimal and is usually computed empirically following
243 Priestly and Taylor (1972). While the prototype E_p does indeed converge toward E as soil
244 moisture increases, there is in fact no unique value of E_{wet} because of the decline E at high soil
245 moisture.

246 As PS09 further note, plotting potential evapotranspiration and evapotranspiration against
247 soil moisture (or a similar variable) may mask the linear nature of the CR. Thus, Figure 1b
248 depicts E_p directly as a function of E. In this case, the approximate linearity implied by equation
249 (1) is found to hold over a large range of E and E_p values. A linear regressive best fit to the E_p
250 vs. E relationship for $E < 6$ mm day^{-1} yields a slope, i.e., the parameter b in equation (1), of
251 magnitude ~3.8. This value of b is quantitatively consistent with the estimates of Kahler and
252 Brutsaert (2006), Szilagyi (2007), and PS09, and unlike the original treatment of Bouchet (with
253 $b = 1$), implies a strongly asymmetric CR. The implied value of b is close to γ, the
254 dimensionless slope of the saturation specific humidity curve, which is 3.5 in the baseline
255 configuration; in fact, as we show in the parameter sensitivity analyses in Section 4a), b varies
256 predominantly with γ, which is consistent with the theoretical arguments presented in Granger
257 (1989).

258 We can, in fact, derive an analytic expression for the CR for our land-atmosphere coupling
259 prototype. We begin by subtracting γH from E_p and invoke the zero surface flux constraint to
260 yield:

261 $$E_p - \gamma H = E_p + \gamma E - \gamma R_s \quad (9)$$

Then, using the bulk formulae expressions for E_p and H, the left-hand side of (9) can be expanded as

$$E_p - \gamma H = \epsilon_H (a_{1s}\gamma T - b_{1s} q) \tag{10}$$

Since precipitation rate $P = \epsilon_c \big(q - q_c(T)\big)$, q can be eliminated in favor of P, which upon rearranging the terms gives:

$$E_p + \gamma E = \gamma R_s - \frac{b_{1s}\epsilon_H}{\epsilon_c} P + f(T) \tag{11}$$

In (11), $f(T) = \epsilon_H (1+\gamma)^{-1} [a_{1s}\gamma T - b_{1s} q_c(T)]$ is just a function of the (prescribed) tropospheric temperature, and is thus constant over the prototype transect.

Comparing (11) to (2), we find:

$$b = \gamma \tag{12}$$

and

$$E_{wet} = (1+\gamma)^{-1} [\gamma R_s + f(T) - \frac{b_{1s}\epsilon_H}{\epsilon_c} P]. \tag{13}$$

As discussed above, in prior work, E_{wet} was defined using the relationship of Priestley and Taylor (1972). The ~~first term of~~ term $(1+\gamma)^{-1}\gamma R_s$ in equation (13) corresponds to the Priestley-Taylor formulation but with a coefficient of 1 in lieu of α. It is worth noting that Kahler and Brutsaert's *in situ* observations imply a Priestley-Taylor coefficient in the range of 0.89 to 1.13, which is in line with the value of 1 for the coefficient of E_{wet} suggested by (13). The remaining terms in E_{wet} are not explicitly represented in the Priestley-Taylor relationship E_{wet}, although this dependence may be implicitly captured through variation of the Priestley-Taylor coefficient. However, we note that the dependence of equation (13) on precipitation implies a negative feedback of P on the E_{wet}, since higher tropospheric moisture is associated with higher

283 precipitation, thereby decreasing vapor pressure deficit at the surface and suppressing E_{wet}. This
284 is consistent with the decrease to E at high soil moisture evident in Figure 1a.

285 It is obvious that E_{wet} as defined by (13) is not constant across the prototype transect, as
286 it depends on surface radiative heating and precipitation. (In a more general model, variations in
287 tropospheric temperature across the transect would also impact the value of E_{wet}.) Again, we
288 point out that the Priestley-Taylor relationship only shows an explicit dependence on radiation
289 (and the Clausius-Clapeyron slope). In addition to the negative feedback of precipitation on
290 E_{wet} through the vapor deficit, R_{surf} itself also decreases as P increases, owing to the negative
291 cloud-radiative forcing associated with deep convective clouds (see Lintner et al. 2013). Related
292 to the non-constancy of E_{wet}, we also note that value of b differs slightly from the value inferred
293 from directly fitting to the linear portion of the E_p vs. E curve in Figure 1b.

294

295 *3b) Budyko curve*

296 Within our prototype, the steady-state soil moisture equation (6) can be recast as:

297 $$B(\phi) = \left[1 - Q_{runoff}/P\right] \tag{14}$$

298 For the simple case of a land surface bucket model with a runoff power law scaling exponent of
299 $\eta = 2$, and noting that soil moisture can be expressed as $w = \beta(w) = \frac{E}{E_p} = \frac{B(\phi)}{\phi}$, equation (14)
300 reduces to a quadratic equation in $B(\phi)$, with an analytic solution in terms of ϕ expressed as:

301 $$B(\phi) = \frac{\phi^2}{2}\left(\sqrt{1 + \frac{4}{\phi^2}} - 1\right) \tag{15}$$

302 Figure 3 illustrates the Budyko curves for the baseline configuration of the prototype ($\eta = 4$) and
303 the analytic solution for $\eta = 2$, with Budyko's well-known empirical formulation $B(\phi) =$
304 $\sqrt{\phi \tanh(\phi^{-1})(1 - e^{-\phi})}$ for comparison. Also depicted are the energy- and water-limited

asymptotes. For the baseline configuration, $B(\phi)$ at intermediate values of aridity index lies above the empirical Budyko fit, while the $\eta = 2$ curve lies below. Variation in the shape of $B(\phi)$ with increasing values of η is consistent with decreasing runoff for a given value of precipitation, which in turn necessitates shifting the surface water balance to favor E over Q_{runoff}. We point out that equation (15) possesses limiting behavior consistent with empirically-derived estimates in prior studies (Budyko 1961, Fu 1981): thus, $B(\phi) \to 0$ as $\phi \to 0$ with a linear asymptote $B(\phi) \sim \phi$, while and $B(\phi) \to 1$ as $\phi \to \infty$ with an asymptote $B(\phi) \sim 1 - \phi^{-1}$. The limiting behavior of $B(\phi)$ as $\phi \to 0$ further implies that $E \to E_p$, which in turn necessitates $E_p \to 0$ in this limit. In other words, the decline in E at high soil moisture noted in Section 3a is also consistent with the Budyko curve.

4) Parameter and process sensitivity

4a) Parameter sensitivity

We now explore how the CR depends on parameter values assumed in the prototype. In particular, we focus on how the implied slope of E_p vs. E (e.g., the slope of the dashed black line in Figure 1b) depends on a subset of four prototype parameters: the dimensionless slope of the saturation specific humidity curve, γ; the surface drag coefficient, which is embedded in the turbulent flux scaling coefficient ε_H; the surface cloud longwave forcing, c_{surf}; and the convective adjustment timescale, τ_c. Our consideration of γ is motivated by its control on the Bowen ratio or, similarly, the evaporative fraction (Gentine et al. 2011), and thus effectively the relative variation of q compared to Ts. We note that with global warming the saturation specific humidity is expected to increase and thereby modify precipitation and the hydrologic cycle (Held and Soden 2006). The surface drag coefficient depends on surface roughness, which could

account for some of the heterogeneity in the observed slope of E_p vs. E. The remaining two parameters, c_{surf} and τ_c, are associated with two of the more uncertain aspects of current generation climate models, namely the effect of clouds on radiation and the parameterization of deep convection, respectively. Although the representation of clouds and convective processes are grossly simplified in the prototype, we can view the parameter sensitivity to c_{surf} and τ_c as a guide for anticipating how uncertainty in analogues to these parameters contained in more complex climate models may be expected to influence the CR evident in these models.

Figure 4 illustrates the percentage variation of the CR slope relative to its baseline value (~3.8) as functions of percentage variations in each of the four sensitivity parameters. Each of the latter is varied uniformly over a range of ±50% of the baseline values indicated in Table 1. It is immediately clear that the slope of the CR varies in a 1:1 manner with γ. On the other hand, for the remaining three parameters, the percent change in the CR slope is typically an order of magnitude smaller. We point out the nonlinearity associated with changing the surface drag coefficient, as decreasing surface drag produces a proportionately larger reduction in the slope of the CR compared to increasing surface drag by the same amount.

Since γ is just the slope of the Clausius-Clapeyron relationship, it has a quasi-exponential dependence on temperature and thus may be expected to vary sharply across the range of observed terrestrial temperature conditions. One consequence of this dependence is that the CR may be expected to become more asymmetric with warming, as higher values of the slope imply a larger change in E_p for a given change in E. In turn, this may have implications for the strength of the coupling between the land surface and atmosphere in a warming climate. For example, recent work by Dirmeyer et al. (2012, 2013, 2014) points to increases in metrics of

land-atmosphere coupling strength in a warming climate. In section 5, we further explore the response of our prototype to a global warming scenario.

In contrast to the complementary relationship, the Budyko curve exhibits no apparent change in shape for these parameter variations. This shape invariance is unsurprising given that the Budyko curve is only a function of the aridity index ϕ, as can be seen directly in the analytic solution for the analytic solution for $\eta = 2$ (equation 15) or by substituting the expression for runoff in equation (14). Thus, while E, E_p, and P vary in response to changing prototype parameters, their ratios are constrained to lie along a fixed Budyko curve. Yang et al. (2009) suggest such shape invariance is characteristic of the Budyko curve response to what they broadly term "climate conditions," as they note climate forcing at a particular location simply moves the system from one point along its characteristic Budyko curve to another. By contrast, Yang et al. (2009) show how different locations fall onto distinct Budyko curves as a result of land surface or landscape properties such as soil, vegetation cover, rooting depth, etc.

4b) Process intervention experiments

Apart from considering the sensitivity of the CR relationship (or Budyko curves) to parameter values, we can also assess how the prototype solutions respond to altering a particular process or term in the governing equations. For the first such intervention-type experiment, we alter the evapotranspiration (E-intervention experiments) by prescribing as constant either i) β or ii) E_p. E-intervention experiment i) is analogous to the methodology adopted in the Global Land Atmosphere Coupling Experiment (GLACE)-type studies for comparing simulations with and without interactive soil moisture (Koster et al. 2004, 2006, Seneviratne et al. 2006). E-intervention experiment ii) is similar to the approach Lintner et al. (2013) used to sever the

feedback of near surface climate onto E_p, which here is mediated principally through suppression of the dependence of potential evapotranspiration on "atmospheric drying power", since the variation of radiative forcing across the prototype transect in its baseline configuration is weak (see discussion below).

Rather than present the complementary relationship for the E-intervention experiments (since the CR necessarily breaks down in either case), we instead show Ts and q as functions of w (Figures 5a and 5b, respectively). For E-intervention experiment i) with β prescribed, the variation in Ts across soil moisture conditions (gray curve) is considerably reduced: while the difference in the baseline Ts (black curve) between the driest and wettest conditions is roughly 5K, it is under 0.5K with β prescribed. Similarly, the range of variation in specific humidity (here scaled to its surface value) across soil moisture states is attenuated relative to the baseline, although it is less pronounced than for surface temperature. Qualitatively opposite behavior is seen under E-intervention experiment ii) with E_p prescribed, as the variations of both Ts and q across the range w are increased relative to their baseline values. Note that at low soil moisture, the behavior of the baseline case more closely resembles E_p prescribed experiments, while at high soil moisture, it is more similar to the β prescribed experiment.

We can further assess how the CR changes with intervention in either surface sensible heat H or surface radiative heating R_s, by prescribing either of these fluxes to a constant value. Under R_s-intervention (Figure 6a), there is little net change in the CR relative to the baseline over most of the range of soil moisture; however, at high w, both E_p and E are slightly increased. The increase in E_p arises through a slight elevation of surface radiation heating above the baseline state, since the negative effect of cloud shortwave forcing, i.e., more convective clouds leading to less surface shortwave heating, is absent. This in turn feeds back onto precipitation, which is

396 slightly enhanced. We further mention a competing effect, namely increased surface longwave
397 forcing (and hence warming) with increased water vapor and convective cloudiness. For the
398 parameter values chosen, this effect loses out to the shortwave forcing. On the other hand,
399 uncertainty in these parameter values, particularly the cloud forcing, could alter the balance of
400 these two effects.

401 Under H-intervention (Figure 6b), the CR is dramatically altered, as E_p drops off more
402 rapidly with increasing soil moisture, while E rises faster at low soil moisture and then flattens
403 off. The quantitative details of the change in shape of E_p and E depend on the value of sensible
404 heat flux prescribed. Plotting E_p vs E (not shown) yields a best fit linear regressive slope of ~28,
405 consistent with the very asymmetric nature of the CR when the variation in H across the transect
406 is suppressed.

407

408 **5) Impacts of global warming and large-scale irrigation**

409 *5a) Global warming*

410 How the hydrologic cycle responds to global warming is clearly of great significance to
411 projecting climate change impacts (Allen and Ingram 2002, Milly et al. 2005). At present, our
412 understanding of the hydrologic cycle response to warming is guided by some theoretical
413 constraints, e.g., the Clausius-Clapeyron relationship promotes enhanced tropospheric
414 moistening, although model projections show considerable spread in the regional signatures of
415 hydrologic cycle change (Held and Soden 2006; Neelin et al. 2013). Assessing global warming
416 impacts on the terrestrial hydrologic cycle is complicated by changes in land use such as
417 deforestation and agricultural conversion and coupling to vegetation (Lee et al. 2011).

418 Over the latter half of the 20th century, several studies have reported widespread decreases in
419 pan evaporation (Lawrimore and Peterson 2000; Hobbins et al. 2004; Roderick and Farquhar
420 2004; Shen et al. 2009), which can be related to E_p. Several hypotheses have been proposed to
421 explain the decreasing trend in pan evaporation, including increasing precipitation reducing the
422 vapor pressure deficit of the lower atmosphere, global dimming reducing shortwave radiative
423 heating at the surface, and stilling of surface winds reducing the exchange coefficient. Van
424 Heerwaarden et al. (2010) conducted an extensive set of sensitivity tests for each of these effects
425 on the CR using a conceptual model of the diurnal terrestrial boundary layer. They concluded
426 that "except over wet soils, the actual evapotranspiration is more sensitive to changes in soil
427 moisture than to changes in short wave radiation so that global evaporation should have
428 increased. Nevertheless, Wild et al. (2004) speculate that in the latter half of the 20th century,
429 increased moisture transport from the oceans enhanced precipitation over land, but suppressed
430 the evaporation—opposite to [their] expectations".

431 Figure 7 depicts the effect on prototype hydroclimate of imposing a 2K warming of the
432 prescribed column-mean temperature. In this figure, differences between the 2K warming
433 configuration and the baseline are plotted against baseline values of w; also shown is the
434 difference in soil moisture between the 2K warming and baseline scenarios. Across the range of
435 baseline soil moisture conditions, the imposed warming decreases E_p (black), since q itself
436 increases. While E (gray) increases with warming at w, it decreases for $w > 0.5$, which is
437 consistent with the results of van Heerwaarden et al. (2010). In addition, P (blue) increases under
438 warming over the entire range of precipitation values (similar to Wild et al. 2004), albeit with a
439 local minimum at intermediate soil moisture values.

The opposing changes of E_p and E with warming at low soil moisture are consistent with expectations from the CR, as an increase in one corresponds to a decrease in the other. Of course, increasing the temperature increases the value of γ, which means the slope of the CR increases between the baseline and 2K warming scenarios. On the other hand, since E_{wet} decreases with tropospheric warming, both E_p and E follow the behavior of E_{wet} and therefore decrease.

While the values of hydroclimatic variables may change substantially between the baseline and 2K warming scenarios, the Budyko curve is unaltered, as discussed in Section 4a. However, as Figure 8 illustrates, forcing conditions, i.e., the value drying advection, identified with specific points along the Budyko curve in the baseline scenario are shifted to lower values of the aridity index ϕ in the 2K warming scenario, since E_p decreases while P increases. Based on these results, we note the potential utility of the Budyko curve in providing qualitative or even quantitative constraints on how terrestrial hydroclimate variables will respond to warming.

5b) Large-scale irrigation

Over many parts of the world, irrigation has been adopted to support agricultural production. Over India, for example, irrigation is now sufficiently extensive that large-scale alterations of hydroclimate may be occurring (Cook et al. 2010, Guimberteau et al. 2011). With respect to potential irrigation-induced changes in hydroclimate, Ozdogan et al. (2006) employed a mesoscale climate model and field data to demonstrate that large-scale irrigation in southeastern Turkey has impacted evaporation and potential evaporation in a complementary manner. They found a variety of interactions responsible for the trends, including increased atmospheric stability, decreased vapor pressure deficit, and, interestingly, a strong decrease in wind speed. Han et al. (2014) point out that while trends in E_p have often been invoked to estimate possible

463 trends in E, how irrigation may impact E_p has typically been neglected in assessment and
464 interpretation of E_p trends. It is thus worth briefly investigating how large-scale irrigation
465 modulates the Budyko and complementary relationships within the framework of the prototype
466 analyzed here. To do this, we consider the addition of an irrigation source, I, to the soil moisture
467 balance equation (6), which then becomes $P + I = E + Q_{runoff}$.

468 To see the impact of irrigation on the prototype hydroclimate, Figure 9 depicts E, E_p, and P
469 in the baseline and $I = 2$ mm day^{-1} configurations. Here we have plotted these quantities with
470 respect to both horizontal dry advection (Figure 9a) and soil moisture (Figure 9b). Given the
471 direct moistening of the atmosphere by irrigation, the transition between nonprecipitating and
472 precipitating conditions in the presence of irrigation occurs at a significantly larger value of
473 drying advection in the large-scale irrigation scenario, as shown in Figure 9a. Across the range
474 of moisture advection values, both E and P are enhanced in the presence of large-scale irrigation,
475 as expected, and E_p decreases, in line with complementarity. Additionally, at low to
476 intermediate precipitation, E exceeds P. Thus, whatever soil moisture is not locally recycled as
477 precipitation would instead be transported downwind, as suggested by some studies on observed
478 irrigation (e.g., DeAngelis et al. 2010). Viewed with respect to soil moisture (Figure 9b), the
479 inclusion of large-scale irrigation is seen to induce a slight increase in E for a given value of w.
480 On the other hand, since the value of drying advection is larger at a given w in the presence of
481 irrigation, E_p itself is larger. Directly relating E_p to E indicates effectively no change in the slope
482 of the CR, though the intercept is increased when irrigation is applied (not shown). Precipitation
483 at a given value of w is lowered in the irrigated scenario.

484 As a consequence of the changes in E and P, the Budyko curve for irrigated conditions
485 (Figure 10, dotted line) is shifted above its baseline: in fact, the irrigated Budyko curve extends

above 1 for $\phi > 1$, as water limitation is effectively alleviated with the imposed irrigation water source. When E is replaced by the residual $E^* = E - I$, the resulting Budyko-like curve (stars) drops below the baseline.

Of course, we should point out that by imposing irrigation in the prototype with tropospheric temperature prescribed, we are neglecting a potentially important cooling of the lowermost atmosphere, not to mention that our prototype does not account for changes in convective initiation or triggering that may occur, e.g., through changes to atmospheric stability. Moreover, we do not take into account vegetation control on E since we only represent soil moisture dependence of evapotranspiration through a bucket model. Thus, the irrigation impacts described here merely reflect the direct effect of added moisture to the atmosphere.

6. Summary and conclusions

In this study, we use an idealized prototype incorporating the key physics of large-scale land-atmosphere coupling to derive analytic expressions for the well-known Budyko and complementary relationships. Our approach differs from previous analytic approaches in that precipitation and moisture convergence are treated implicitly rather than applied as an external forcing. The analytic solutions permit straightforward diagnosis of the sensitivity of the Budyko and complementary relationships to atmospheric and land surface parameters. In particular, the slope of the CR is shown to be mostly dependent on the temperature with important implications for the continental hydrologic cycle with a warming climate. One consequence of this dependence is that the CR may be expected to become more asymmetric with warming, as higher values of the slope imply a larger change in potential evaporation for a given change in evapotranspiration. On the other hand the Budyko curve is very stable to many parameterization

of the model parameters or global temperature. It is thus expected that the Budyko curve should remain relatively stable under a warming climate. Other causes of anthropogenic changes such as large-scale irrigation are however shown to strongly impact the Budyko curve with little impact on the CR.

Acknowledgements

This work was supported by National Science Foundation (NSF) grant AGS-1035968 and New Jersey Agricultural Experiment Station Hatch grant NJ07102.

References Cited

Allen, M. R., and W. J. Ingram, 2002: Constraints on future changes in climate and the hydrologic cycle. *Nature, 419*, 224–232. doi:10.1038/nature01092.

Betts, A. K., J. Ball, A. Beljaars, M. J. Miller, and P. Viterbo, 1996: The land surface-atmosphere interaction: A review based on observational and global modeling perspectives. *J. Geophys. Res.-Atmos.*, *101*(D3), 7209–7225.

Betts, A. K., J. H. Ball, M. Bosilovich, P. Viterbo, and Y. Zhang, 2003: Intercomparison of water and energy budgets for five Mississippi subbasins between ECMWF reanalysis (ERA-40) and NASA Data Assimilation Office GCM for 1990 *Journal of Geophysical Research: Atmospheres (1984–2012)* 108 (D16)

Betts, A. K., and P. Viterbo, 2005: Land-surface, boundary layer, and cloud-field coupling over the southwestern Amazon in ERA-40. *J. Geophys. Res.-Atmos.*, *110*(D14), 1–15. doi:10.1029/2004JD005702.

Betts, A. K., 2007: Coupling of water vapor convergence, clouds, precipitation, and land-surface processes. *J. Geophys. Res.-Atmos.*, *112*(D10), D10108. doi:10.1029/2006JD008191.

Betts, A. K., 2014: Coupling of winter climate transitions to snow and clouds over the Prairies, *J. Geophys. Res.-Atmos* (in press)

Bosman, H. H., 1987: The influence of installation practices on evaporation from Symon's tank and American Class A-pan evaporimeters. *Agr. For. Meteor., 41*, 307–323.

Bouchet, R., 1963: Evapotranspiration reelle et potentielle, signification climatique. *IAHS Publ., 62*, 134– 142.

Brutsaert, W., and H. Stricker, 1979: An advection-aridity approach to estimate actual regional evapotranspiration. *Water Resour. Res., 15*, 443– 450.

Brutsaert, W., and M. B. Parlange, 1998: Hydrologic cycle explains the evaporation paradox. *Nature, 396*, 29– 30.

Budyko, M., 1961: *The heat and water balance of the Earth's surface, the general theory of physical geography and the problem of the transformation of nature*, Soviet Geography: Review and Translation.

Budyko, M.I., 1974: *Climate and life*. Academic Press, Orlando, FL, 508 pp.

Cook, B. I., M. J. Puma, and N. Y. Krakauer, 2010: Irrigation induced surface cooling in the context of modern and increased greenhouse gas forcing. *Clim. Dyn.*, *37*, 1587–1600, doi:10.1007/s00382-010-0932-x.

565 Crago, R., and R. Crowley, 2005: Complementary relationships for near-instantaneous
566 evaporation. *J. Hydrol., 300*, 199–211, doi:10.1016/j.jhydrol.2004.06.002.
567
568 DeAngelis, A., F. Dominguez, Y. Fan, A. Robock, M. D. Kustu, and D. Robinson, 2010:
569 Evidence of enhanced precipitation due to irrigation over the Great Plains of the United States. *J.*
570 *Geophys. Res., 115*, D15115, doi:10.1029/2010JD013892.
571
572 Dirmeyer, P. A., B. A. Cash, J. L. I. Kinter, C. Stan, T. Jung, L. Marx, L. et al., 2012: Evidence
573 for Enhanced Land-Atmosphere Feedback in a Warming Climate. *J. Hydrometeor.*, *13*, 981–995.
574 doi:10.1175/JHM-D-11-0104.1.
575
576 Dirmeyer, P. A., Y. Jin, B. Singh, and X. Yan, 2013: Trends in land-atmosphere interactions
577 from CMIP5 simulations. *J. Hydrometeor.* 14 (3) doi:10.1175/JHM-D-12-0107.1.
578
579 Dirmeyer, P. A., Z. Wang, M. J. Mbuh, and H. E. Norton, 2014: Intensified land surface control
580 on boundary layer growth in a changing climate. *Geophys. Res. Lett.*,
581 doi:10.1002/2013GL058826
582
583 Donohue, R. J., M. L. Roderick, and T. R. McVicar, 2007: On the importance of including
584 vegetation dynamics in Budyko's hydrological model. *Hydrol Earth Syst Sc*, *11*, 983–995.
585
586 Eagleson, P., 1978a: Climate, soil, and vegetation 2. The distribution of annual precipitation
587 derived from observed storm sequences. *Water Resour Res*. *14*(5), 713-721
588
589 Eagleson, P., 1978b: Climate, soil, and vegetation, 6. Dynamics of the annual water balance.
590 *Water Resour Res 14*(5), 749-764
591
592 Eagleson, P., 1978c: Climate, soil, and vegetation. 1. Introduction to water balance dynamics.
593 *Water Resour Res 14*(5), 705-712
594
595 Fu, B. P., 1981: On the calculation of the evaporation from land surface (in Chinese), *Sci. Atmos.*
596 *Sin., 5*, 23–31.
597
598 Gentine, P., D. Entekhabi, D., and J. Polcher, 2011. The Diurnal Behavior of Evaporative
599 Fraction in the Soil-Vegetation-Atmospheric Boundary Layer Continuum. *J. Hydrometeor.*, *12*,
600 1530–1546. doi:10.1175/2011JHM1261.1
601
602 Gentine, P., P. D'Odorico, B. R. Lintner, G. Sivandran, and G. Salvucci, 2012: Interdependence
603 of climate, soil, and vegetation as constrained by the Budyko curve. *Geophys. Res. Lett., 39*,
604 L19404, doi:10.1029/2012GL053492.
605
606 Gerrits, A. M. J., H. H. G. Savenije, E. J. M. Veling, and L. Pfister, 2009: Analytical derivation
607 of the Budyko curve based on rainfall characteristics and a simple evaporation model. *Water*
608 *Resour. Res.*, *45*, doi:10.1029/2008WR007308.
609

610 Granger, R. J., 1989: A complementary relationship approach for evaporation from nonsaturated
611 surfaces. *J. Hydrol., 111*, 31– 38.
612
613 Guimberteau, M., K. Laval, A. Perrier, and J. Polcher, 2011. Global effect of irrigation and its
614 impact on the onset of the Indian summer monsoon. *Clim. Dyn.*, *39*, 1329–1348.
615 doi:10.1007/s00382-011-1252-5
616
617 Han, S., Q. Tang, D. Xu and S. Wang, 2014: Irrigation-induced changes in potential evaporation:
618 more attention is needed. *Hydrol. Process., 28*, 2717–2720. doi: 10.1002/hyp.10108.
619
620 Harman, C. J., P. A. Troch, and M. Sivapalan, 2011: Functional model of water balance
621 variability at the catchment scale: 2. Elasticity of fast and slow runoff components to
622 precipitation change in the continental United States. *Water Resour. Res.*, *47*,
623 doi:10.1029/2010WR009656.
624
625 Held, I. M., and B. J. Soden, 2006: Robust response of the hydrological cycle to global warming.
626 *J. Clim., 19*, 5686—5699.
627
628 Hobbins, M. T., J. A. Ramirez, T. C. Brown, and L. H. J. M. Claessens, 2001: The
629 complementary relationship in estimation of regional evapotranspiration: The complementary
630 relationship area evapotranspiration and advection-aridity models. *Water Resour. Res., 37*,
631 1367—1387.
632
633 Hobbins, M. T., J. A. Ramirez, and T. C. Brown, 2004: Trends in pan evaporation and actual
634 evapotranspiration across the conterminous US: Paradoxical or complementary? *Geophys. Res.*
635 *Lett.*, *31*, doi:10.1029/2004GL019846.
636
637 Istanbulluoglu, E., T. Wang, O. M. Wright, and J. D. Lenters, 2012: Interpretation of hydrologic
638 trends from a water balance perspective: The role of groundwater storage in the Budyko
639 hypothesis. *Water Resour. Res.*, *48*, doi:10.1029/2010WR010100.
640
641 Kahler, D. M., and W. Brutsaert, 2006: Complementary relationship between daily evaporation
642 in the environment and pan evaporation, *Water Resour. Res.*, *42*, doi:10.1029/2005WR004541.
643
644 Kleidon, A., and M. Heimann, 1998: A method of determining rooting depth from a terrestrial
645 biosphere model and its impacts on the global water and carbon cycle. *Global Change Biol.*,
646 *4*(3), 275–286.
647
648 Koster, R., and M. Suarez, 1999: A simple framework for examining the interannual variability
649 of land surface moisture fluxes. *J Clim.*, *12*, 1911–1917.
650
651 Koster, R.D., and co-authors, 2004: Regions of strong coupling between soil moisture and
652 precipitation. *Science, 305*, 1138–1140.
653
654 Koster, R. D., and co-authors, 2006: GLACE: The Global Land-Atmosphere Coupling
655 Experiment. Part I: Overview. *J. Hydrometeor.*, *7*, 590–610.

Kirchner, J. W., 2009: Catchments as simple dynamical systems: Catchment characterization, rainfall-runoff modeling, and doing hydrology backward. *Water Resour. Res.*, *45*, W02429, doi:10.1029/2008WR006912.

Lawrimore, J., and T. Peterson, 2000: Pan evaporation trends in dry and humid regions of the United States, *J Hydrometeor.*, *1*, 543–546.

Lee, J.-E., B.R. Lintner, C.K. Boyce, and P.J. Lawrence, 2011: Land use change exacerbates tropical South American drought by sea surface temperature variability. *Geophys Res. Lett., 38*, L19706, doi:10.1029/2011GL049066.

Lettau, H., 1969: Evapotranspiration Climatonomy. I. A New Approach to Numerical Prediction of Monthly Evapotranspiration, Runoff, and Soil Moisture Storage. *Mon. Weather Rev.*, *97* (10), 691–699.

L'homme, J., and L. Guilioni, 2006: Comments on some articles about the complementary relationship. *J. Hydrol.*, *323*, 1–3, doi:10.1016/j.jhydrol.2005.08.014.

Lintner, B.R., P. Gentine, K.L. Findell, F. D'Andrea, A.H. Sobel, and G.D. Salvucci, 2013: An idealized prototype for large-scale land-atmosphere coupling. *J. Clim., 26*, 2379—2389, doi:10.1175/JCLI-D-11-000561.1

Manzoni, S., G. Vico, G. Katul, P. A. Fay, W. Polley, S. Palmroth, and A. Porporato, 2011: Optimizing stomatal conductance for maximum carbon gain under water stress: a meta-analysis across plant functional types and climates. *Funct. Ecol.*, *25*, 456–467, doi:10.1111/j.1365-2435.2010.01822.x.

Milly, P. C. D., 1994: Climate, soil water storage, and the average annual water balance. *Water Resour. Res., 30*, 2143–2156.

Milly, P. C. D., and K. Dunne, 2002: Macroscale water fluxes - 2. Water and energy supply control of their interannual variability. *Water Resour Res*, *38*, doi:10.1029/2001WR000760.

Milly, P. C. D., K. Dunne, and A. V. Vecchia, 2005: Global pattern of trends in streamflow and water availability in a changing climate. *Nature, 438*, 347–350. doi:10.1038/nature04312.

Morton, F. I., 1983: Operational estimates of areal evapotranspiration and their significance to the science and practice of hydrology*, J. Hydrol.,* 66*,* 1–76*.*

Neelin, J.D., and N. Zeng, 2000: A quasi-equilibrium tropical circulation model—formulation. *J. Atmos. Sci.*, *57*, 1741–1766.

Neelin, J. D., M. Munnich, H. Su, J. Meyerson, and C. Holloway, 2006: Tropical drying trends in global warming models and observations. *Proc. Nat. Acad. Sci., 103*, 6110—6115.

Ozdogan, M., G. Salvucci, and B. Anderson, 2006: Examination of the Bouchet-Morton complementary relationship using a mesoscale climate model and observations under a progressive irrigation scenario. *J Hydrometeor.*, *7*, 235–251.

Pettijohn, J. C., and G. D. Salvucci, 2009: A new two-dimensional physical basis for the complementary relation between terrestrial and pan evaporation. *J. Hydrometeorol., 10*, 565–574, doi:10.1175/2008JHM1026.1.

Porporato, A., F. Laio, L. Ridolfi, and I. Rodríguez-Iturbe, 2001: Plants in water-controlled ecosystems: active role in hydrologic processes and response to water stress - III. Vegetation water stress. *Adv. Water Resour.*, *24*, 725–744.

Porporato, A., E. Daly, and I. Rodríguez-Iturbe, 2004: Soil water balance and ecosystem response to climate change. *Am. Nat*. *164*, 625–632.

Potter, N., L. Zhang, P. Milly, T. McMahon, and A. Jakeman, 2005: Effects of rainfall seasonality and soil moisture capacity on mean annual water balance for Australian catchments. *Water Resour. Res.*, *41*, XX, doi:10.1029/2004WR003697.

Priestley, C. H. B., and R. J. Taylor, 1972: On the Assessment of Surface Heat Flux and Evaporation Using Large-Scale Parameters. *Mon Wea. Rev.*, *100*, 81–88.

Ramirez, J. A., M. T. Hobbins, and T. C. Brown, 2005: Observational evidence of the complementary relationship in regional evaporation lends strong support for Bouchet's hypothesis. *Geophys. Res. Lett., 32*, L15401, doi:10.1029/2005GL023549.

Roderick, M. L., and G. D. Farquhar, 2004: Changes in Australian pan evaporation from 1970 to 2002. *Int. J. Climatol.*, *24*, 1077–1090, doi:10.1002/joc.1061.

Roderick, M. L., and G. D. Farquhar, 2011: A simple framework for relating variations in runoff to variations in climatic conditions and catchment properties. *Water Resour. Res.*, *47*, doi:10.1029/2010WR009826.

Seneviratne, S. I., and co-authors, 2006: Soil moisture memory in AGCM simulations: Analysis of global land-atmosphere coupling experiment (GLACE) data. *J. Hydrometeor.*, *7*, 1090–1112.

Shen, Y., C. Liu, M. Liu, Y. Zeng, and C. Tian, 2009: Change in pan evaporation over the past 50 years in the arid region of China. *Hydrol. Process*, doi:10.1002/hyp.7435.

Sherwood, S., and Q. Fu, 2014: A drier future? *Science, 343*, 737—739, doi:10.1126/science.1247620.

Sivapalan, M., M. A. Yaeger, C. J. Harman, X. Xu, and P. A. Troch, 2011: Functional model of water balance variability at the catchment scale: 1. Evidence of hydrologic similarity and space-time symmetry. *Water Resour. Res.*, *47*, doi:10.1029/2010WR009568.

748 Sobel, A. H., and C. S. Bretherton, 2000: Modeling tropical precipitation in a single column. *J.*
749 *Clim.*, *13*, 4378–4392.
750
751 Sobel, A., J. Nilsson, and L. Polvani, 2001: The weak temperature gradient approximation and
752 balanced tropical moisture waves. *J. Atmos. Sci.*, *58*, 3650–3665.
753
754 Szilagyi, J., 2001: On Bouchet's complementary hypothesis. *J. Hydrol.*, *246*, 155–158.
755
756 Szilagyi, J., 2007: On the inherent asymmetric nature of the complementary relationship of
757 evaporation. *Geophys. Res. Lett., 34*, L02405, doi:10.1029/2006GL028708.
758
759 Szilagyi, J., and J. Jozsa, 2009: Complementary relationship of evaporation and the mean annual
760 water-energy balance. *Water Resour. Res.*, *45*, doi:10.1029/2009WR008129.
761
762 Troch, P. A., G. F. Martinez, V. R. N. Pauwels, M. Durcik, M. Sivapalan, C. Harman, P. D.
763 Brooks, H. Gupta, and T. Huxman, 2009: Climate and vegetation water use efficiency at
764 catchment scales. *Hydrol. Process*, *23*, 2409–2414, doi:10.1002/hyp.7358.
765
766 Tuttle, S.E., and G.D. Salvucci, 2012: A new method for calibrating a simple, watershed-scale
767 model of evapotranspiration: maximizing the correlation between observed streamflow and
768 model-inferred storage. *Water Resour. Res., 48*, W05556, doi:10.1029/2011WR011189
769
770 van Heerwaarden, C. C., J. Vilà-Guerau de Arellano, and A. J. Teuling, 2010: Land-atmosphere
771 coupling explains the link between pan evaporation and actual evapotranspiration trends in a
772 changing climate. *Geophys. Res. Lett., 37*, L21401, doi:10.1029/2010GL045374.
773
774 Wild, M., A. Ohmura, H. Gilgen, and D. Rosenfeld, 2004: On the consistency of trends in
775 radiation and temperature records and implications for the global hydrological cycle, Geophys.
776 Res. Lett., 31, L11201, doi:10.1029/2003GL019188.

777 Williams, C. A., and co-authors, 2012: Climate and vegetation controls on the surface water
778 balance: Synthesis of evapotranspiration measured across a global network of flux towers.
779 *Water Resour. Res.*, *48*, W06523, doi:10.1029/2011WR011586.
780
781 Yang, D., F. Sun, Z. Liu, Z. Cong, G. Ni, and Z. Lei, 2007: Analyzing spatial and temporal
782 variability of annual water-energy balance in nonhumid regions of China using the Budyko
783 hypothesis. *Water Resour. Res.*, *43*, W04426, doi:10.1029/2006WR005224.
784
785 Yang, D., W. Shao, P. J.-F. Yeh, H. Yang, S. Kanae, and T. Oki, 2009: Impact of vegetation
786 coverage on regional water balance in the nonhumid regions of China. *Water Resour. Res., 45*,
787 W00A14, doi:10.1029/2008WR006948.
788
789 Yang, H., D. Yang, Z. Lei, and F. Sun, 2008: New analytical derivation of the mean annual
790 water-energy balance equation. *Water Resour. Res.*, *44*, doi:10.1029/2007WR006135.
791
792 Zanardo, S., C. Harman, P. Troch, P. Rao, P., et al. 2012: Intra-annual rainfall variability control
793 on interannual variability of catchment water balance: A stochastic analysis. *Water Resour. Res*.

48, W00J16, doi:10.1029/2010WR009869

Zeng, N., J.D. Neelin, and C. Chou, 2000: A quasi-equilibrium tropical circulation model–Implementation and simulation. *J. Atmos. Sci.*,, *57*, 1767–1796.

Zhang, L., K. Hickel, W. Dawes, F. Chiew, A. Western, and P. Briggs, 2004: A rational function approach for estimating mean annual evapotranspiration. *Water Resour. Res.*, *40*, W02502, doi:10.1029/2003WR002710.

802 **Table and Figure Captions**

803 **Table 1:** Parameter definitions and values in the baseline land-atmosphere coupling prototype.

804 **Figure 1:** Complementary relationship in the baseline configuration. a) Potential
805 evapotranspiration (E_p; black), evapotranspiration (E; gray), and precipitation (P; blue) as
806 functions of soil moisture (w). b) E_p vs. E (black) and the 1:1 line (gray). Also shown is the
807 best fit linear regression of the E_p to E relationship (squares).

808 **Figure 2:** Baseline complementary relationship compared to Kahler and Brutsaert's
809 observational data from the Little Washita River basin in Oklahoma, USA (c.f., Figure 5 in
810 Kahler and Brutsaert, 2006). Symbols shown correspond to two different normalizations of the
811 observations and gray lines to best fits through these points. The values along the abscissa, E_{MI},
812 correspond to the ratio of actual to pan evaporation in Kahler and Brutsaert (2006) and are
813 identical to soil moisture in the prototype. Prototype E_p and E (red and purple curves, respective)
814 have been normalized with respect to the value of E_{wet} corresponding to the maximum value of
815 E along the transect.

816 **Figure 3**: Prototype Budyko curves for the baseline prototype, i.e., $\eta = 4$, in the formulation of
817 runoff (thick black), for equation (15) for $\eta = 2$ (gray), and Budyko's empirical formula
818 (squares). The dashed lines are the energy- and water-limited asymptotes.

819 **Figure 4:** Parameter sensitivity of the complementary relationship slope. Results shown are for
820 varying: the slope of the saturation specific humidity with respect to temperature (no symbols),
821 surface drag coefficient (circles), surface cloud radiative forcing (stars), and convective
822 adjustment timescale (squares).

823 **Figure 5:** Comparison of prototype (a) surface temperature Ts and (b) surface air humidity qa
824 for the baseline (black), fixed β (gray), and fixed E_p (blue) configurations of the prototype. Note
825 that qa is converted to temperature units of K.

826 **Figure 6:** Impact on the complentary relationship from prescribing either (a) net surface
827 radiative heating or (b) sensible heat flux. The curves depicted correspond to E_p (black), E
828 (gray), and P (blue) for the baseline configuration (solid) and prescribed radiative or sensible
829 heat fluxes (dashed).

830 **Figure 7:** Differences in E_p (black), E (gray), and P (blue) for a +2K warming relative to the
831 baseline configuration as functions of soil moisture in the baseline configuration. Also shown is
832 the difference in soil moisture (dashed black), which has been rescaled by a factor of 10.

833 **Figure 8:** Shift in selected points along the Budyko curve for the baseline (black symbols) and
834 +2K warming (red) configuration. Pairs of like shaped symbols correspond to the same level of
835 imposed drying advection forcing. The values shown in the inset are the percentage changes for
836 each of the baseline and +2K warming pairs.

837 **Figure 9:** Large-scale irrigation impacts on prototype hydroclimate. a) E_p (black), E (gray), and
838 P (blue) for the baseline (solid curves) and $I = 2$ mm day^{-1} large-scale irrigation scenario (dotted

curves), plotted with respect to horizontal moisture advection, scaled to units of mm day^{-1}. Here, horizontal advection values correspond to drying advection, which are associated with decreasing precipitation. b) As in a), but with soil moisture as the abscissa.

Figure 10: Comparison of Budyko curves for the baseline (solid) and $I = 2$ mm day^{-1} (dotted) configurations. Also shown is a Budyko-like curve in which E is replaced by $E^* = E - I$ (stars).

Table 1: Parameter definitions and values in the baseline land-atmosphere coupling prototype

Parameter	***Definition***	***Value***
a_{1s}	Weighting factor for surface temperature	0.30
α	Priestley-Taylor coefficient	1.26
b_{1s}	Weighting factor for surface moisture	1.15
b	Complementary relationship scale factor	--
c_{surf}	Surface cloud longwave forcing coefficient	0.18
γ	Dimensionless slope of Clausius-Clapeyron relationship	3.5
ε_H	Linearized surface turbulent flux scaling coefficient	42 mm day^{-1} K^{-1}
η	Runoff power law scaling exponent	4
τ_c	Convective adjustment timescale	2 hours

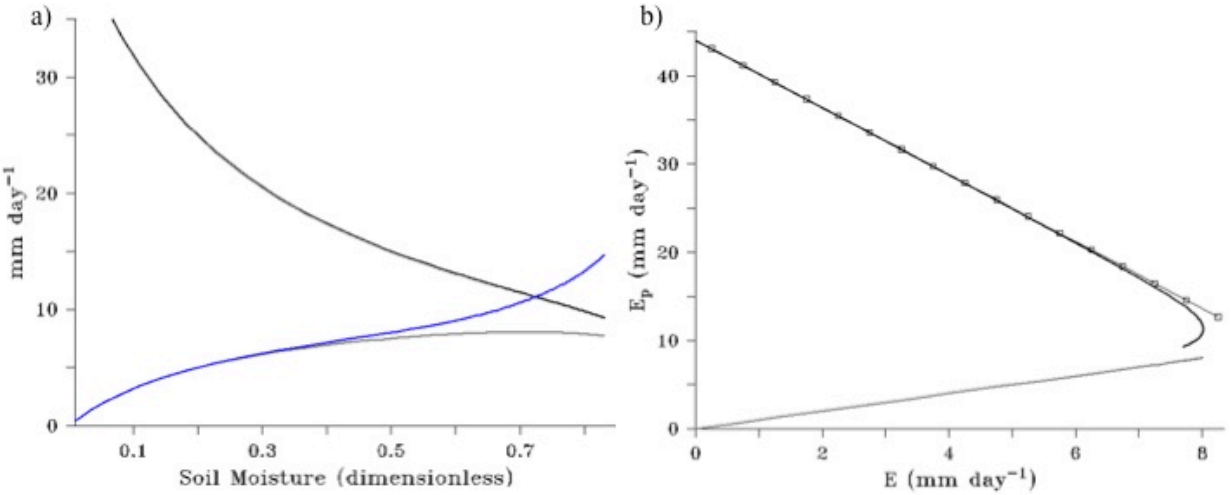

Fig. 1: Complementary relationship in the baseline configuration. a) Potential evapotranspiration (E_p; black), evapotranspiration (E; gray), and precipitation (P; blue) as functions of soil moisture (W). b) E_p vs. E (black) and the 1:1 line (gray). Also shown is the best fit linear regression of the E_p to E relationship (squares).

847

848

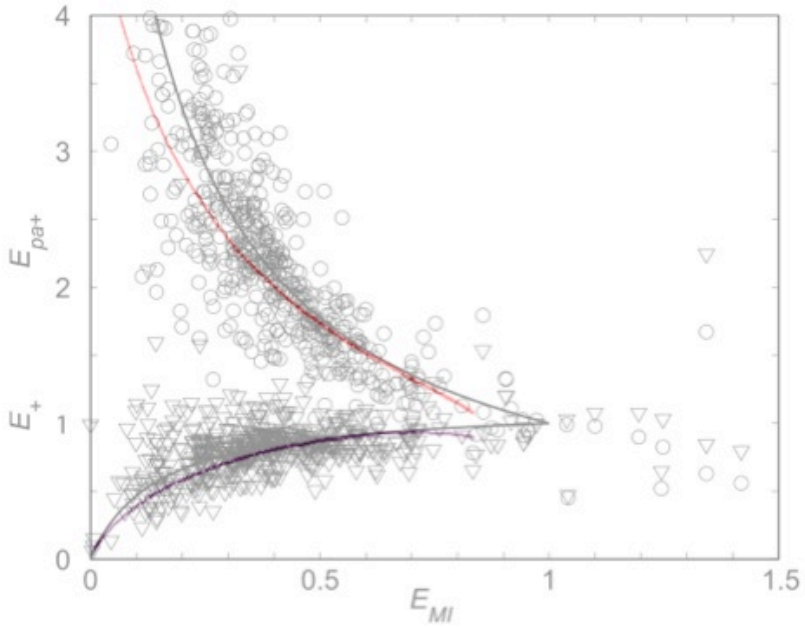

Fig. 2: Baseline complementary relationship compared to Kahler and Brutsaert's observational data from the Little Washita River basin in Oklahoma, USA (c.f., Figure 5 in Kahler and Brutsaert, 2006). Symbols shown correspond to two different normalizations of the observations and gray lines to best fits through these points. The values along the abscissa, E_{MI}, correspond to the ratio of actual to pan evaporation in Kahler and Brutsaert and are identical to soil moisture in the prototype. Prototype E_p and E (red and purple curves, respective) have been normalized with respect to the value of E_{wet} corresponding to the maximum value of E along the transect.

849

850

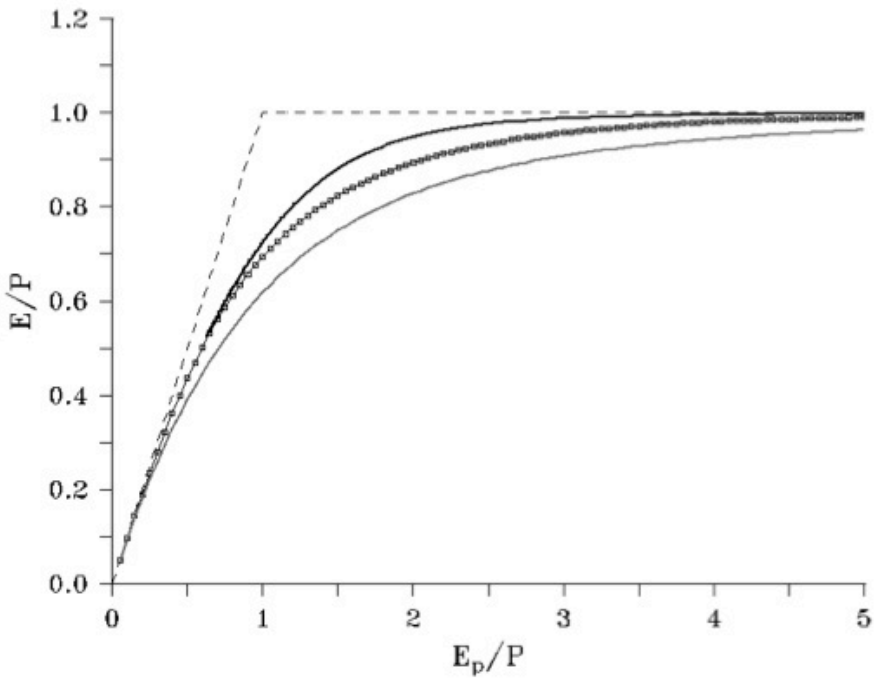

Fig. 3: Prototype Budyko curves for the baseline prototype, i.e., $\eta = 4$ in the formulation of runoff (thick black), for equation (15) for $\eta = 2$ (gray), and Budyko's empirical formula (squares). The dashed lines are the energy- and water-limited asymptotes.

851

852

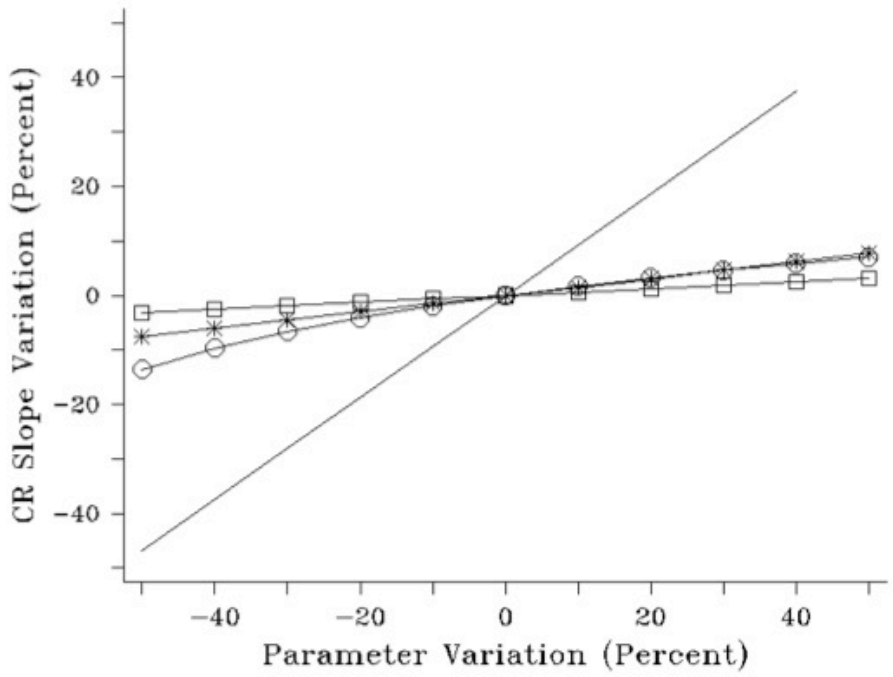

Fig. 4: Parameter sensitivity of the complementary relationship slope. Results shown are for varying: the slope of the saturation specific humidity with respect to temperature (no symbols), surface drag coefficient (circles), surface cloud radiative forcing (stars), and convective adjustment timescale (squares). Values show along both the abscissa and ordinate are percentages relative to the baseline parameter value and baseline slope, respectively.

853

854

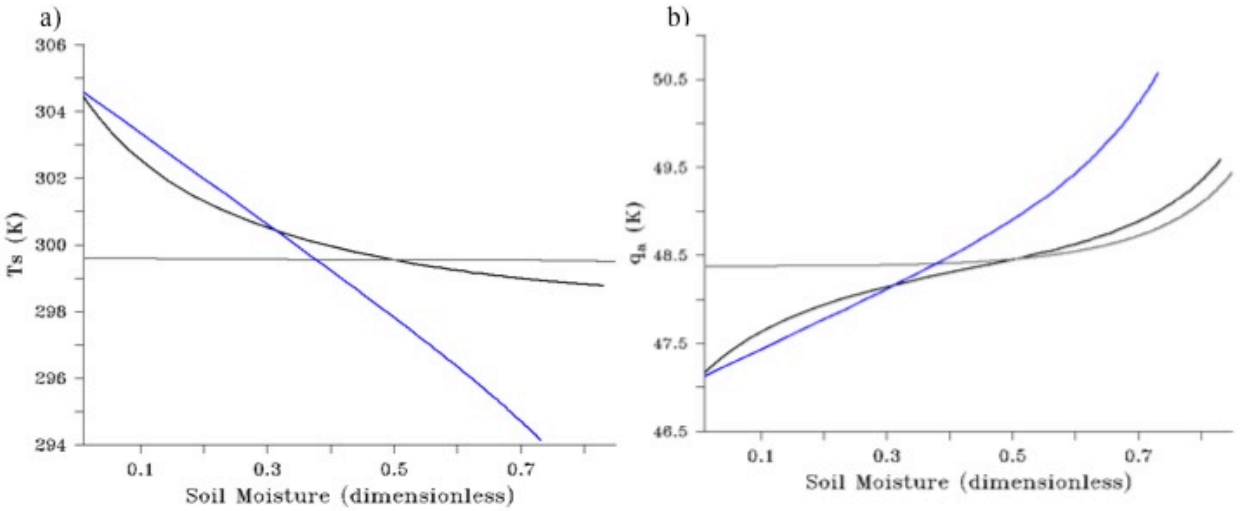

Fig. 5: Comparison of prototype (a) surface temperature *Ts* and (b) surface air humidity *qa* for the baseline (black), fixed β (gray), and fixed Ep (blue) configurations of the prototype. Note that *qa* is converted to temperature units of K.

855

856

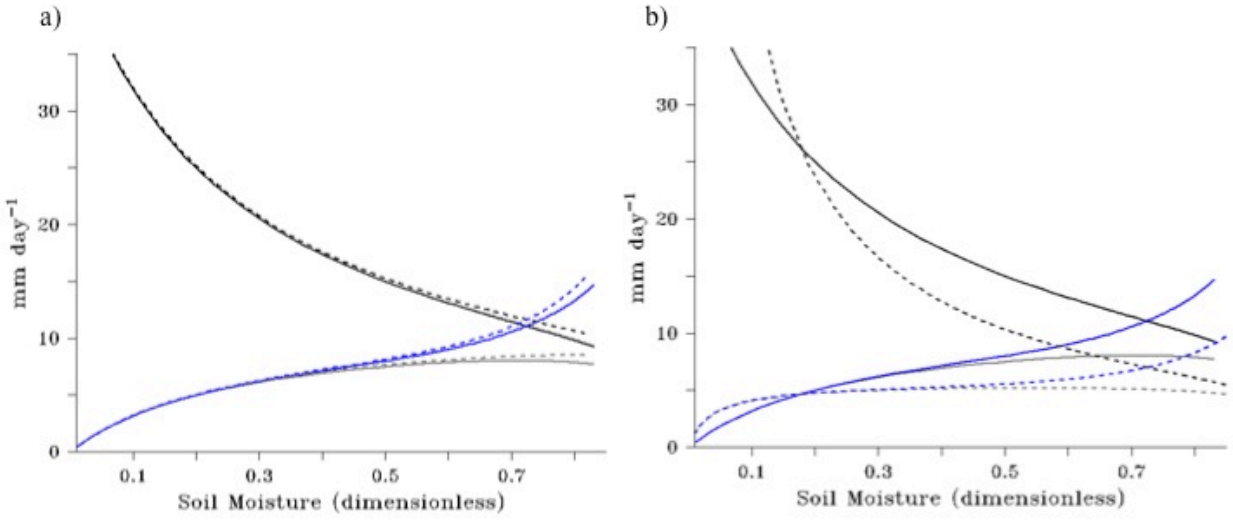

Fig. 6: Impact on the complentary relationship from prescribing either (a) net surface radiative heating or (b) sensible heat flux. The curves depicted correspond to Ep (black), E (gray), and P (blue) for the baseline configuration (solid) and prescribed radiative or sensible heat fluxes (dashed).

857

858

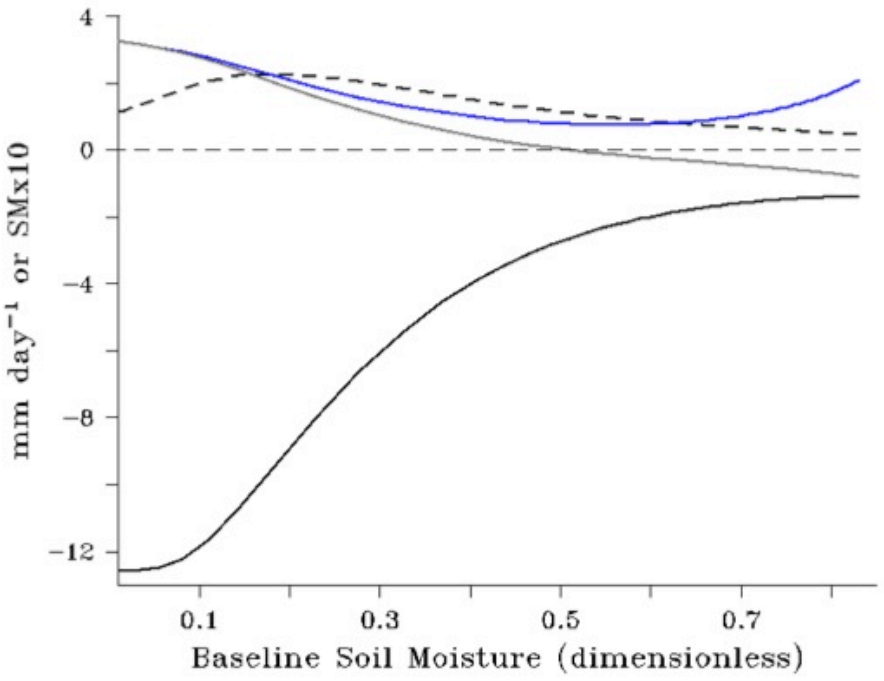

Fig. 7: Differences in E_p (black), E (gray), and P (blue) for a +2K warming relative to the baseline configuration as functions of soil moisture in the baseline configuration. Also shown is the difference in soil moisture (dashed black), which has been rescaled by a factor of 10.

859

860

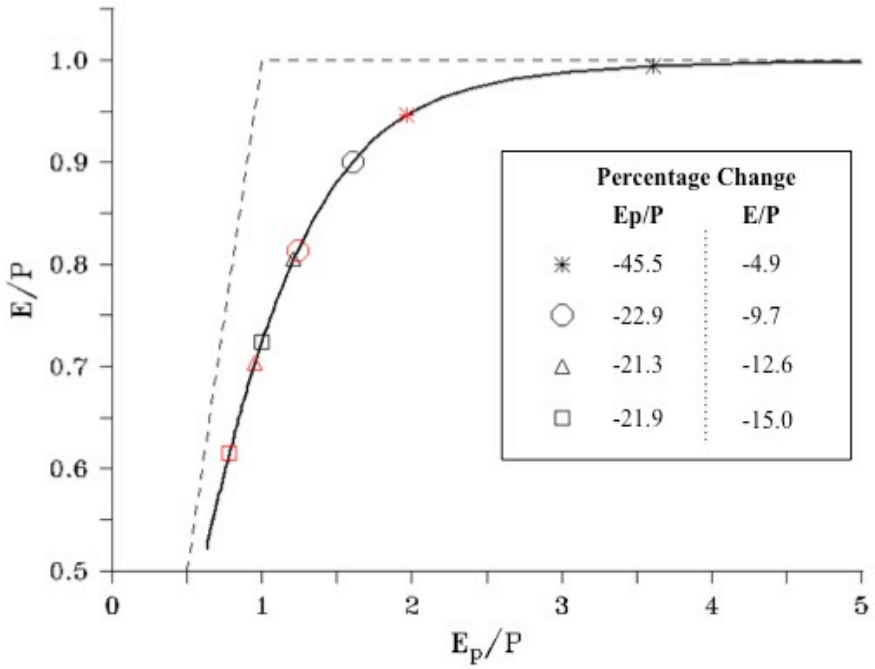

Fig. 8: Shift in selected points along the Budyko curve for the baseline (black symbols) and +2K warming (red) configuration. Pairs of like shaped symbols correspond to the same level of imposed drying advection forcing. The values shown in the inset are the percentage changes for each of the baseline and +2K warming pairs.

861

862

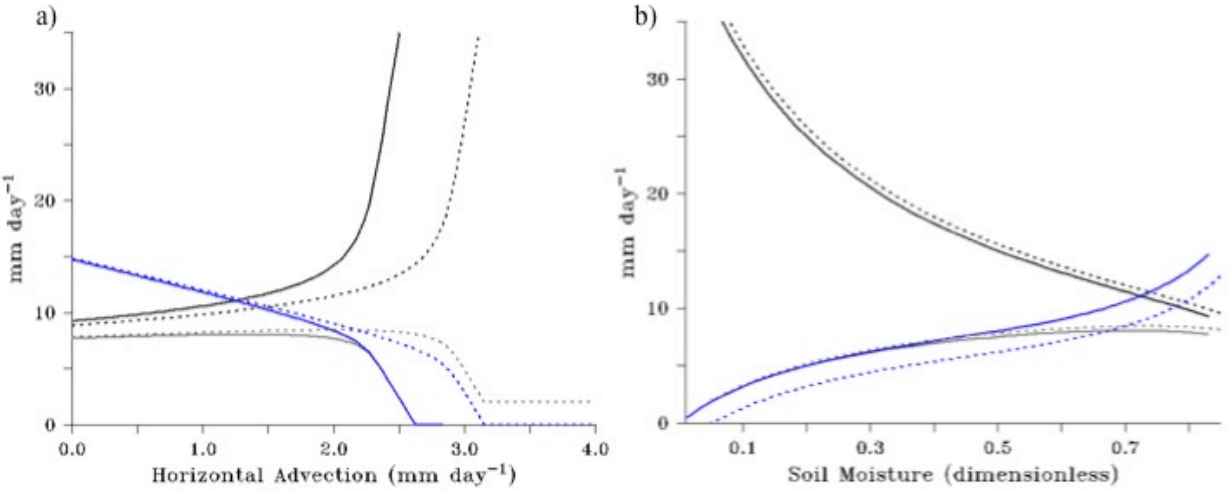

Fig. 9: Large-scale irrigation impacts on prototype hydroclimate. a) E_p (black), E (gray), and P (blue) for the baseline (solid curves) and I = 2 mm day^{-1} large-scale irrigation scenario (dotted curves), plotted with respect to horizontal moisture advection, scaled to units of mm day^{-1}. Here, horizontal advection values correspond to drying advection, which are associated with decreasing precipitation. b) As in a), but with soil moisture as the abscissa.

863

864

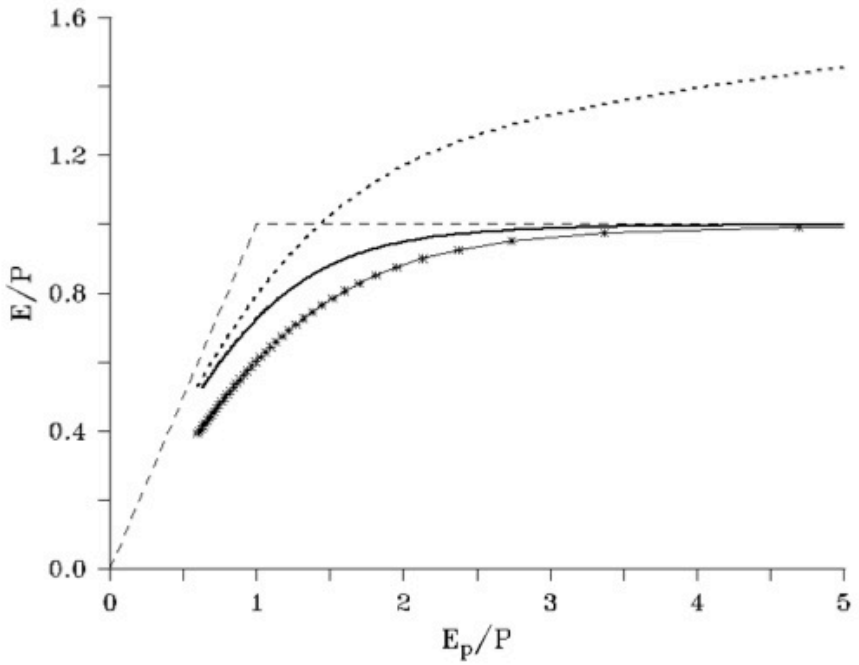

Fig. 10: Comparison of Budyko curves for the baseline (solid) and I = 2 mm day^{-1} (dotted) configurations. Also shown is a Budyko-like curve in which E is replaced by $E^* = E - I$ (stars).

865